

THE MOYJIL SITE, SOUTH-WEST VICTORIA, AUSTRALIA: FIRE AND ENVIRONMENT IN A 120,000-YEAR COASTAL MIDDEN — NATURE OR PEOPLE?

JIM M. BOWLER¹, DAVID M. PRICE², JOHN E. SHERWOOD³ AND STEPHEN P. CAREY⁴

¹School of Earth Sciences, The University of Melbourne, Melbourne, Victoria 3010, Australia

²School of Earth and Environmental Sciences, University of Wollongong, Wollongong, NSW 2520, Australia

³School of Life and Environmental Sciences, Deakin University, PO Box 423, Warrnambool, Victoria 3280, Australia

⁴School of Science, Engineering and Information Technology, Federation University Australia, Ballarat, Victoria 3353, Australia

Correspondence: Jim Bowler, jbowler@unimelb.edu.au

ABSTRACT: At Moyjil (Point Ritchie), a cliffed site at the mouth of the Hopkins River at Warrnambool, south-eastern Australia, an erosional disconformity of Last Interglacial age on both a rock stack and the adjacent headland represents a surface of possible human occupation. Shells of edible marine molluscs occur on the disconformity, together with a distinctive population of transported stones derived from a calcrete of MIS 7 age and bearing variable dark grey to near-black colouration suggestive of fire. Experimental fire produced similar thermal alteration of calcrete. A strong correlation exists between intensity and depth of dark staining on one hand and increased magnetic susceptibility on the other. Thermal luminescence analyses of blackened stones provide ages in the MIS 5e range, 100–130 ka, consistent with independent stratigraphic evidence and contemporaneous with the age of the surface on which they lie. The distribution of fire-darkened stones is inconsistent with wildfire effects. Two hearth-like features closely associated with the disconformity provide further indications of potential human agency. The data are consistent with the suggestion of human presence at Warrnambool during the Last Interglacial.

Keywords: Interglacial sea level, human occupation, magnetic susceptibility, thermoluminescence

A marine shell deposit at Point Ritchie (also known by its Traditional Owner name, Moyjil), the western headland of the Hopkins River at Warrnambool, south-eastern Australia, has been the subject of a long research program. First investigated in 1981 by the late Edmund Gill in association with John Sherwood, this feature has long suggested the possibility of human agency (Sherwood et al. 1994; Nair & Sherwood 2007).

Exposed by post-glacial marine erosion, the site lies on cliffs along the high-energy coastline of southern Victoria (Figure 1) at the seaward margin of the Last Interglacial (LIG) coastal barrier dune, the Dennington Member (Reeckmann & Gill 1981). A small stack (West Stack) of aeolian calcarenite with a horizontal surface area of approximately 40 m² stands some 20 m seaward of the cliffed headland (Figures 1–4). On the headland cliff-top, erosion has cut a narrow platform 2 to 4 m wide into the calcareous deposits of successive coastal dune systems (Bridgewater Formation; Reeckmann & Gill 1981; VandenBerg 2009) belonging to Marine Isotope Stages (MIS) 7 and 5 (Sherwood et al. 2018b). The platform is developed on an ancient (LIG) surface, designated Ground surface alpha, G α (Carey et al. 2018), an erosional disconformity separating groundwater calcrete of MIS 7 from the MIS 5 aeolianite cover. These features are exhumed on both the headland and West Stack.

At some 8 m above present sea level, the stack surface contains an unusual assemblage of marine shells and discoloured stones. At the equivalent level on the headland is a larger accumulation of disrupted and, in many cases, dislodged calcrete and reddish Bridgewater calcarenites. Irregular blocks and stones of various shapes and sizes display an array of distinctive surface darkening, sometimes nearly black.

The association of rock darkening with shells of edible marine species (Sherwood et al. 2018a) high on West Stack presents a challenging complication to an investigation of possible human agency. While many processes may be involved in forming dark rock surfaces (weathering, algal or other biological films), the common agency of fire, if verified here, would add an entirely new complexion to understanding of the site with potentially major implications for the role of people. Does the rock darkening represent fire and, if so, what sort of fire, i.e. is darkening of natural or human agency?

Commencing with an early 2007 working liaison (between JMB and JES), JMB's pursuit of answers to that question forms the substance of this report. It involves examination of stones on West Stack and on the nearby headland platform, supported by evidence from some collapsed blocks. Three methods are used to evaluate the transformation of pale calcrete to darker examples.

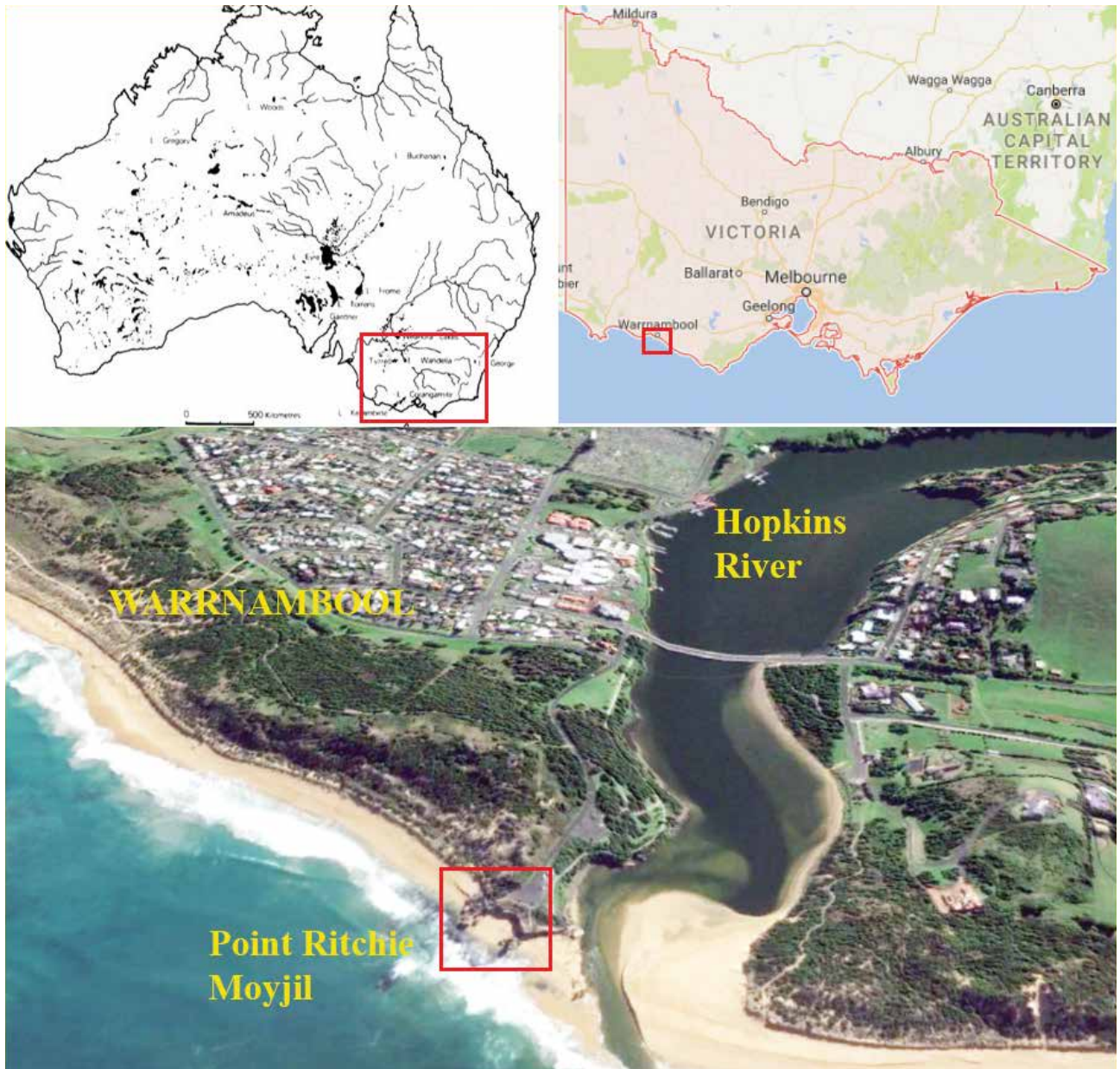


Figure 1: Location of the Point Ritchie/Moyjil site on the southern Victorian coastline at Warrnambool. Oblique aerial from Google Earth. For inset enlargement, see Figure 2.



Figure 2: Study site, aerial enlargement of inset, Figure 1 (Photo: D. Ierodiaconou). West Stack (North & South) separated by some 20 m from the headland. Cliff-top exposures of two calcretes, Rcp groundwater calcrete of penultimate (~200 ka) high sea-level age overlain by sediments and soil calcrete of Last Interglacial age, Qs. Red markers identify location of possible fireplaces in western and eastern locations. See text for discussion.



Figure 3: Panorama of coastline locating West Stack–Headland cliffing. Surface of West Stack finds correlative level bench at +8 m on headland. Note gap between stack and headland carrying cobble beach at toe of boulder slope to headland cliff. Displaced blocks B and D as per Figures 10A & B.

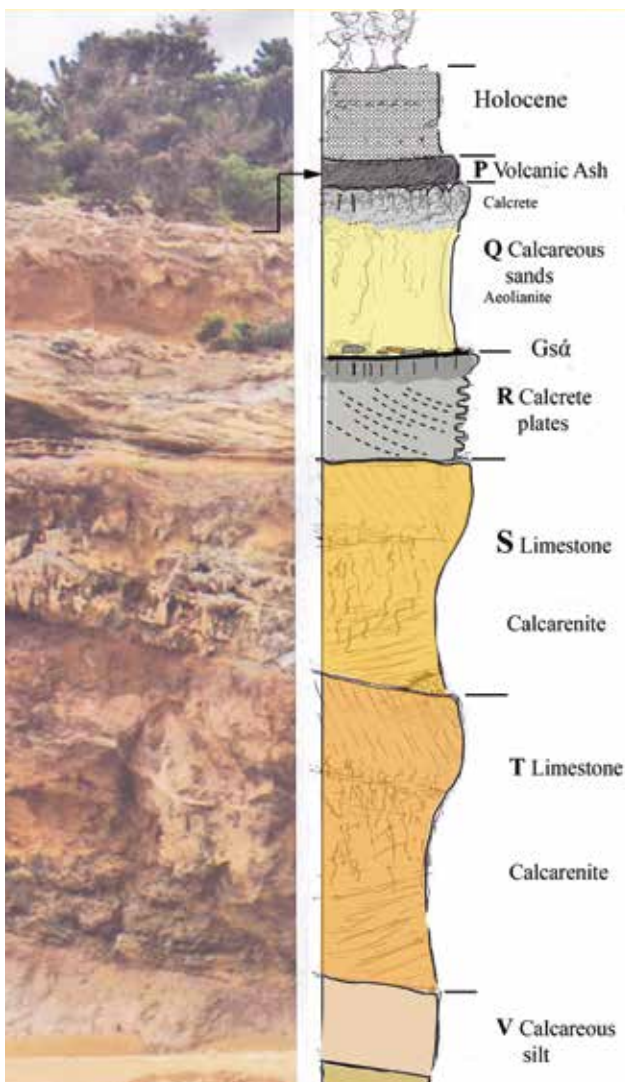


Figure 4: Vertical section through cliffed exposures of Late Quaternary high sea-level units of Bridgewater Formation overlain by volcanic ash of the 35 ka Tower Hill eruption. For details, see Carey et al. (2018) and text herein.

Analytical techniques include:

1. Heating originally pale calcrete in a wood fire
2. Measurement of magnetic susceptibility across the range of calcrete from pale and undarkened to nearly black samples
3. Thermoluminescence (TL) analysis of blackened stones to test the possibility of thermal resetting of parent calcrete.

Detailed analysis of stone and fire evidence follows presentation of the wider stratigraphic and geomorphic context within which such evidence occurs.

STRATIGRAPHY

Vertical cliffs (to 8 m high and 100 m long, Figure 3) at the mouth of the Hopkins River expose outcrop oriented largely east–west and 60 m long, and facing the sea to the south (South Face, Figure 2). A second segment, 40–50 m long, forms the western margin of the Hopkins estuary (East Face, Figure 2).

The geomorphic context and the stratigraphic succession (Carey et al. 2018) are summarised in Table 1 and Figures 4 and 5. The sequence is developed upon the Bridgewater Formation (Upper Pleistocene) aeolianites (dune limestones) and superimposed palaeosols widely developed around the coast of southern and western Australia (Brooke 2001; Murray-Wallace & Woodroffe 2014). The informal system of five units (designated V at the base, T, S, R and Q) record a eustatically controlled history spanning at least the last 400 ka of coastal aeolianite deposition and alternating with soil development (Table 1).

Unit R, MIS 7 age (~220 ka), includes a prominent groundwater calcrete (Rcp) at its base and disconformably overlies units S and T. Erosion of basal unit R exposes groundwater calcrete at an erosional surface designated Ground surface alpha (Gsa).

Gsa is at 8 m Australian Height Datum (AHD) on the headland, where the bench is 2–4 m wide (Figure 5). It carries discoloured stones on the headland and mixed stones and shells on West Stack, often in disorderly arrangement.

rossa has created a second disconformity, Ground surface beta (Gsβ) exposing calccrete Qcs which, according to OSL analysis (Sherwood et al. 2018b), formed after the LIG around 50–60 ka. A possible mass-flow deposit of calccrete blocks and occasional shells, perhaps related to seismicity, is identified on top of Gsβ.

In summary, the site records an unusual coincidence of three highstand Bridgewater units before the MIS 7 phase marked by deposition of the unit R aeolianites and groundwater calccrete, Rcp, on which most of the shell and fire evidence is located. Probably spanning more than 400 ka, the succession of up to six sea-level oscillations at this coastline has left a rich but highly complex record of erosional and depositional features. Our immediate interest is with the upper units of the stratigraphic succession at Moyjil that provide the key to understanding Late Pleistocene environmental change.

GEOMORPHOLOGY

The main elements of geomorphic interest at Moyjil have been introduced by Carey et al. (2018) in the stratigraphic story. Specific features that provide the context for the wide distribution of darkened stones require elaboration here.

On the assumption that darkened stones preserve the legacy of fire, questions of age and environments of formation remain to be defined. In terms of age, the record of sea-level change provides a starting point. The evidence for possible seismic disturbance, labelled the ‘Z-event’ (Carey et al. 2018), provides an additional point of reference. These two processes, sea-level change and possible seismic activity, help calibrate the temporal and spatial context within which the legacy of fire may be explored. This section examines the evidence from several exposures to help refine that framework.

Site locations

The cliffed coastline retains three main areas from which data are derived:

- West Stack blocks (West Stack North — WsN, and West Stack South — WsS), the main shell site with limited occurrences of darkened stone (Figure 8)
- the headland cliff and platform, with many darkened stones but no shell directly on the platform
- an assemblage of fallen blocks.

Spatial and temporal elements of these sites (Figure 5) are central to the matter of darkening and potential fire.

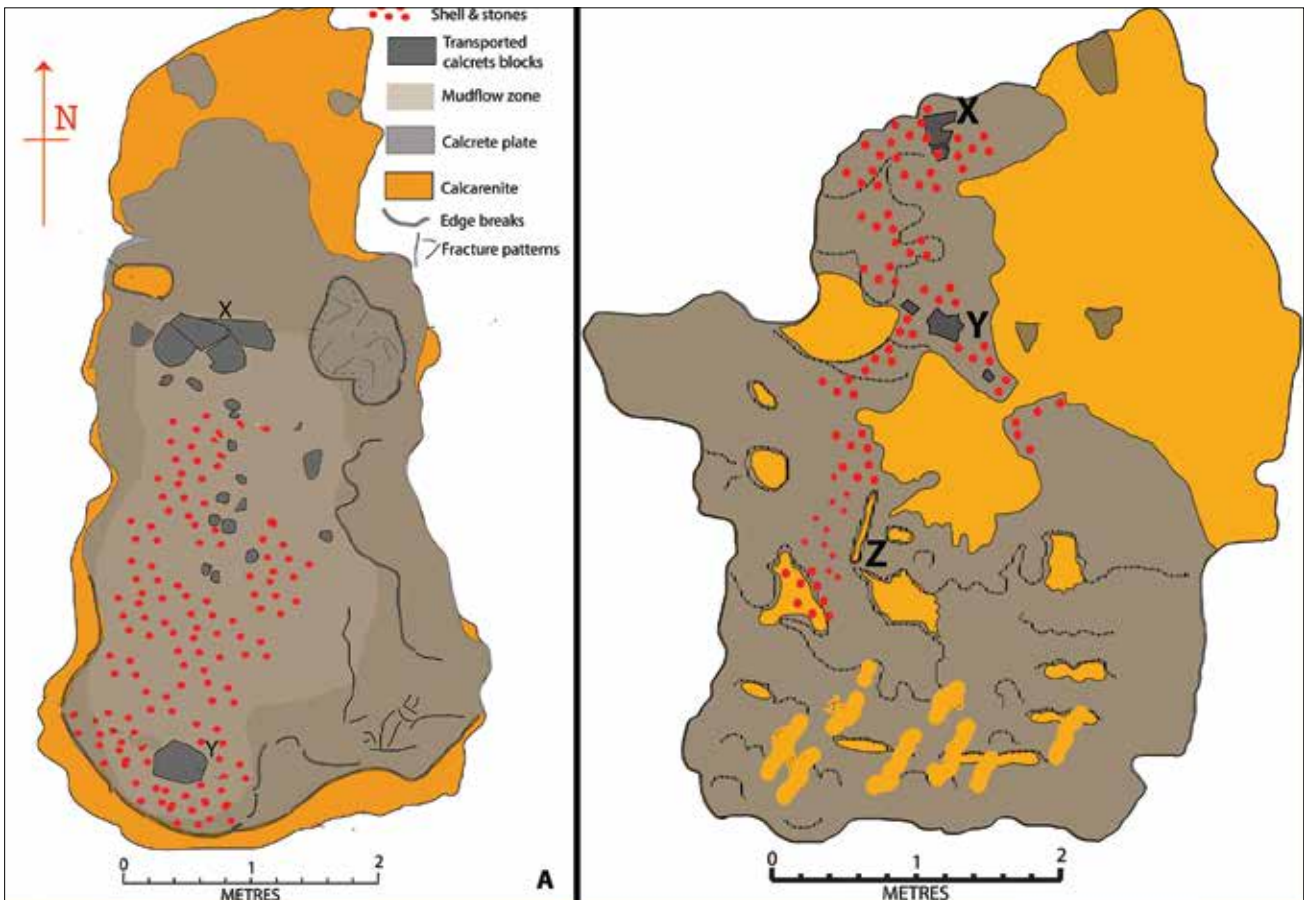


Figure 6: Mapped surfaces of West Stack North (left) and West Stack South (right) showing eroded calccrete cover over unit T calcarenite. Note north to south distribution of shell-stone assemblage over calccrete extending into southern erosion pits, Z on South Stack. X and Y are transported blocks mobilised by major disturbance (the Z event; see text).

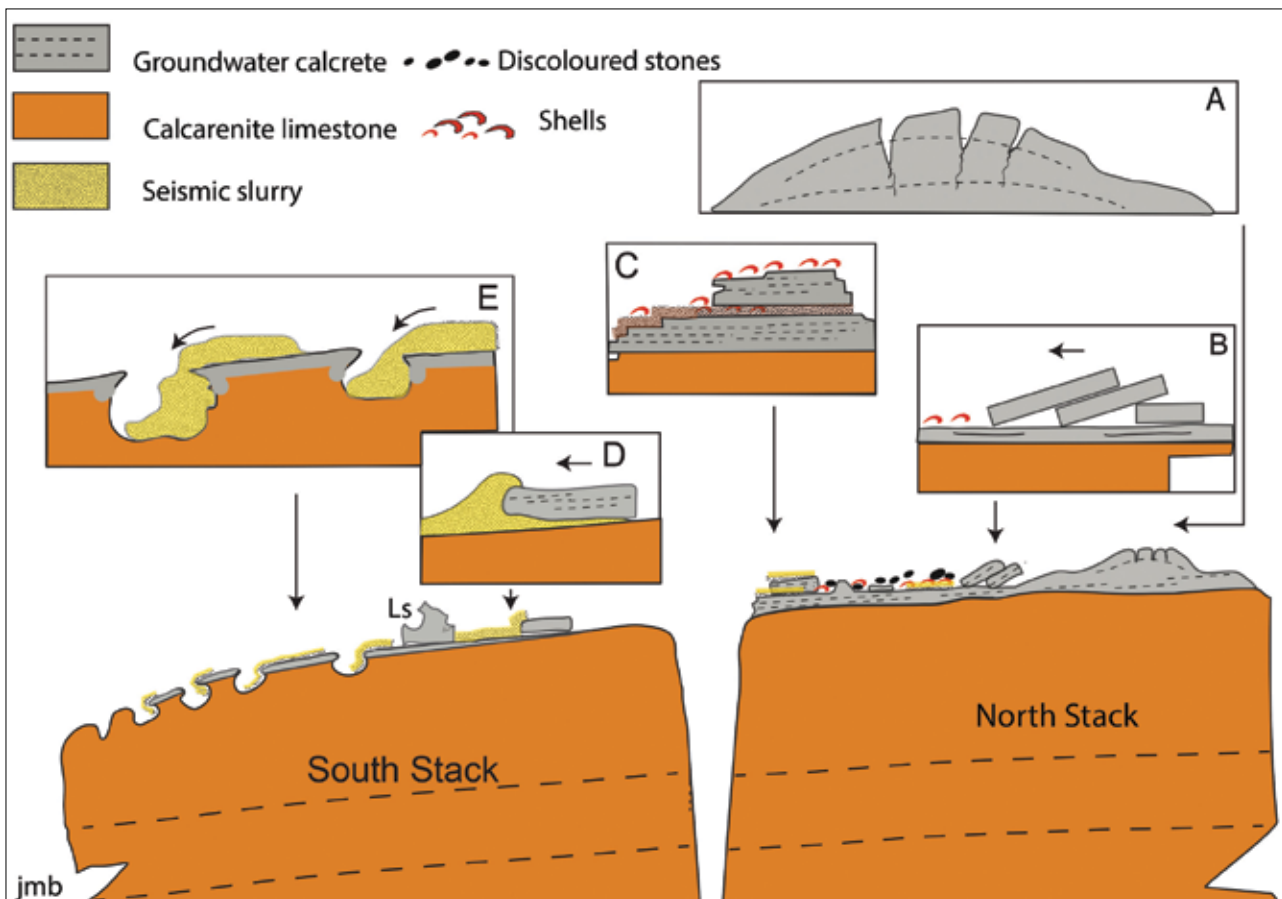


Figure 7: Enlargement of West Stack surface showing stratigraphic layering, pre-calcrete etch pits Ls, large (30–40 cm) irregular limestone erratic, fractured and mobilised calcrete plates in collision with fluidised transport of stone-shell debris, the latter extending into South Stack pre-calcrete etch pits. See also Carey et al. (2018).

- A. Domed calcrete showing radial fractures cemented in place.
 B. Dislodged cemented calcrete plates over-thrusting each other adjacent to Site A.
 C. Dislodged angular calcrete block thrust over shell debris.
 D. Intersection of dislodged a calcrete block with collision effect meeting fluidised calcarenite mudflow with shell fragments.
 E. Erosion pits on the southern sector, South Stack, with transported cemented shell debris.



Figure 8: West Stack scatter of shell fragments with stained calcarete stones lying within layer of transported calcarete debris, features of substantial surface disturbance by possible seismic shock (the Z event).

Although West Stack and the headland are separate today, evidence from West Stack suggests that a connection existed at the time of initial shell collection and stone darkening. The geological complexity of the shell and fire history (discussed in Carey et al. 2018) is addressed here on a site-by-site basis as a prelude to identification of age and environmental factors. A major erosional surface is common to both sites.

Ground surface alpha (G α). Truncating elements of all three sites (WsS, WsN and headland), the erosional surface was formed by LIG highstand erosion of unit R to form a platform-cliff topography at that time (Figure 9). In all three areas, it has exposed layers of unit R groundwater calcrete (Rcp) now strongly fractured by an event attributed to seismic shock. Marine shells and darkened stones, the objects of this study, lie on it.

West Stack. G α occurs on the two formerly connected but now tilted West Stack blocks, WsN and WsS (Figure 6). They stand separated from the headland platform by a



Figure 9: View to north-west across headland platform bench (Rcp calcrete) carrying fractured and redistributed calcrete blocks. Small cliff on right with surface calcrete of unit Q. Red marker locates site of possible fire place, Fp1.

ridge of some 20 metres on which lie irregular calcarenite and calcrete blocks. The combined upper surface of WsN and WsS, a relatively small area (40–50 m²) of high complexity, is a key area of study. Darkened stones on this erosion surface range from pebble- to cobble-sized calcrete blocks together with the main shell deposit. Both stack surfaces carry a distinctive array of discoloured, transported stones lying in disordered orientation (Figure 8).

In the stratigraphic context, Rcp calcrete plates disconformably overlie pinkish *terra rossa* horizons of the S–T units. Calcrete cover varies from plates 20–30 mm thick on the NW margin, thinning to the west where small pockets of circular corrosion expose the underlying S–T surface (Figures 6, 7).

The calcrete layer includes zones of intense plate-like fracturing with some blocks dislodged and moved laterally. Towards the north, several such transported blocks have collided with one riding over the other (Figure 7B). These are identified by Carey et al. (2018) as evidence of suspected seismic activity, the Z-event.

Erosional pits and occasional potholes cut into the underlying S–T deposits often feature a lip of unit R calcrete film (Figure 7E). This requires early pothole formation, a feature consistent with major erosion at the

disconformable contact between units R and S during a highstand estimated in the 200–240 ka range (Sherwood et al. 2018b).

On the western margin of WsN a deep notch at the +5 m AHD level infilled by beach and shell detritus (Q1 of Carey et al. 2018) provides evidence of coastal erosion during the LIG (~110–125 ka).

Darkened stones, debris flow. Fragmented marine shells occur with darkened stones especially in the central region of WsN (Figure 6). Patterns of weakly cemented darkened and undarkened stones in a calcareous sandy matrix lie in disorder, suggesting the effects of a major disturbance, the probable Z-event debris flow. As noted by Carey et al. (2018), shell fragments have been transported and selectively sorted by groundwater injection in a north-to-south direction, some reaching the erosional pits on the southern part of WsS (Figure 7E). A catchment source of such waters requires a discharge point north of the present stack which critically implies a connection with the headland at that time.

Two features point towards major changes on West Stack coincident with Z-event disturbances. First, transported shells, blocks and stones (Figure 7B, E) are preserved in a position of mass movement, virtually



Figure 10: Displaced blocks B and D (see Figure 3).

A. Large fallen block, (Block B in Carey et al. 2018) lying on its side on beach sands. Ranging pole held by John Sherwood defines marine abrasion surface ($GS\alpha$) truncating formerly horizontal surface of unit S. Abrasion surface carries remnants of original Rcp calcrete bearing later dark-grey to black staining as well as transported and dark-stained calcrete stones (see Figure 11).

B. Two triangular plates of calcrete Rcp in 'hanging' context lying off main headland platform. Surface mantle of reddish-brown debris matrix over fractured plates carries highly disturbed array of blackened stones.

a photographic record of seismic impact. Second, the absence of any sign of post-disturbance deposition of shells or darkened stones suggests cessation of their formation, be it by human or natural process. By contrast, headland evidence shows continuation of darkened stone generation over a substantial area of the $Gs\alpha$ platform after the major disturbance. Relationships between West Stack and the cliff-platform mainland area require clarification.

Headland cliff and platform. Extending some 20 m north of West Stack, a narrow boulder-strewn ridge truncates units T and V, linking the basal stack to the headland cliff (Figures 3, 5). The ridge rises to the north with a highly irregular cover of metre-sized boulders of dislodged and weathered calcrete, and forms a rampart or talus slope leading to the higher unit Q calcrete surface (Qcs) at 10 to 11 m AHD. The toe of the slope carries an assemblage of rounded calcrete stones with shell fragments (a beach deposit). Lying at +6 m AHD, slightly higher than the +5 m notch, this 'cobble beach' identifies a phase of intermediate shoreline deposition between WsN and the headland. In contrast to fresh fractured blocks fallen onto today's beach, its association with weathered talus boulders suggests a phase of headland cliff instability adjusted to the +6 m sea level of that time.

The basal connecting ridge carrying the cobble beach deposit (Figure 5) forms a relatively low but important topographic feature. Its eastern edge drops to modern beach level beside numerous collapsed blocks, mainly of pinkish unit S and T calcarenite. Further to the east, headland cliffs in the main embayment (Figures 2, 3) rise vertically to join the platform-like exposure of $Gs\alpha$ cutting across Rcp calcrete to eroding unit Q sands (Figures 5,

9). That level, although equivalent to the surface of West Stack, is significantly different. Marine shells, common on the stack, are absent, though the platform carries similar darkened stones.

To clarify the relationship between darkened stones and the $Gs\alpha$ surface on which they lie, the relationship of $Gs\alpha$ with sea level remains to be clarified. Important evidence comes from collapsed blocks.

Blocks. Two items of special interest to the fire history occur detached from their original positions. First, a large fallen block of reddish units S and T (designated Block B, Carey et al. 2018) lies on the modern beach (Figure 10A). Two lines of evidence suggest the effects of fire. A planar surface abrasion, due to marine planation, carries dark grey to near-black stains both directly on the abraded surface and on a population of transported calcrete stones lying on it. The surface displays angular fractures, 10–30 cm deep, cross-cutting surface darkening (Figure 11). Attributed to effects of the Z-event, the fracturing provides a measure of the relative timing of staining. When the block is restored to its original position, the abrasion surface lies at +8 m AHD and defines a sea at that level (Carey et al. 2018).

In the second example, two triangular platy Rcp calcrete blocks (designated Di and Dii,) have partially collapsed but retain basal attachment to the headland (Figure 10B).

The tilted block Dii (Figure 10B) preserves items of special significance. A blanket cover of fine-grained, reddish brown calcarenite over planar fractured calcrete, Rcp, is in turn overlain by an assemblage of darkened stones. Arrayed in positions suggesting mass transport, the stones, with the calcarenite layer and fractured calcrete, provide yet another expression of the Z-event.



Figure 11: Black stain, due to presumed fire on fractured MIS 5 abrasion surface of Block B (Figure 10A). Note sharp-edged block fractures with population of transported stones, many with dark staining. A small rhizomorph with calcrete cover over dark stain, a remnant of unit Q, carbonate deposition.

DISCUSSION

All sites (headland platform, West Stack, Block B) reflect interaction of the two factors, changing sea level and possible seismicity, on the patterns of darkening (? fire) records. On West Stack, the association of marine shells and stone darkening suggests a close association, one with the other. The collection and deposition there of shells require a sea level below the stack surface. Evidence from the marine abrasion surface on Block B is critical.

The restored position of Block B on the cliff at +8 m AHD equates with a LIG shoreline (Carey et al. 2018), equivalent to the MIS 5 sea level as regionally established near 125 ka (Hearty et al. 2007; Murray-Wallace 2002). From topographic data, a sea level of that height would overtop both the headland platform and West Stack. Shell and stone deposition on West Stack clearly post-dates that event and requires a lower sea level. Similarly, the patchy darkening of, and deposition of darkened stones on the +8 m abrasion surface on Block B (Figure 11) reflects a fall in sea level.

On West Stack, no dark stones post-date Z-event debris. By contrast, on the headland continued darkening of stones before and after the Z-event suggests a lack of connection between the two at that time. The proposal of a gap between West Stack and the headland after the Z-event is supported by additional evidence.

A deep infilled wave-cut notch with shell and gravelly clastics on the northern side of WsN at +5 m AHD occurs near the slightly higher cemented ‘cobble beach’ midway between the stack and on the talus slope adjacent to the headland cliff (+6 m AHD, Figures 3, 5). The stack–headland separation was arguably complete for such deposits to form. It coincided with the change in darkening

patterns between sites at that time. The Z-event appears contemporaneous with that change, suggesting a cause-and-effect relationship between them.

Improved chronology. Much stratigraphic importance is attributed to the marine abrasion surface of detached Block B (Carey et al. 2018). Its age depends on the reliability of its restoration to the original cliff. Quite separately, the development of the gap featuring the cobble beach between West Stack and the headland (Figures 3, 5) provides evidence of a +6 m AHD sea level. Furthermore, preservation of the boulder talus, unaffected by any later high sea level, implies that the time of formation of the +6 m level is a minimum age for all of the Z-event, penecontemporaneous shell accumulations and darkening features. The last time the sea reached that level was near 120 ka, providing an independent estimate of age.

Darkening sequence. The data provide a sequential account of potentially fire-produced darkening, sea-level variation and pre- and post-Z disruption effects. Events are summarised in order below, beginning with the maximum sea level of the LIG:

- +8 m AHD sea level, marine abrasion on Block B, top of West Stack and headland platform
- Slight fall in sea level, permitting collection and deposition of shells on West Stack, and darkening on the emerged +8 m AHD abrasion surface
- Major disturbance (?seismic), causing intensive fracturing of calcrete on West Stack and on abrasion surface of Block B
- Hiatus of activity on stack but continuity of darkening (?fire evidence) on headland
- Post-Z-event deposition of +6 m AHD cobble beach and boulder talus between disconnected stack and headland.

The timing of maximum shell and stone darkening (?fire) activity occurred before burial by unit Q, the OSL-dated aeolianite (Sherwood et al. 2018b). These events lie within the relatively short interval between maximum high sea level (~125 ka) and beginning of shoreline retreat (~120 ka).

EVIDENCE OF FIRE

Stones, form and colour

This report on the evidence of fire at Moyjil focuses specifically on stones darkened grey to nearly black. They form a group of special interest within a much larger population of fractured and transported calcrete stones of variable shape and size. What were the environmental conditions necessary to accumulate numerous blackened stones derived from MIS 7 calcrete (Rcp) lying on a surface of MIS 5 age (G α)?

Mixed with shells on West Stack, fractured stones carpet G α . Angular to sub-rounded blocks are frequently >15–20 cm in diameter while more rounded examples are typically <10 cm. Two rock types are represented, pale calcrete (larger blocks and plates) and reddish limestone (smaller blocks) from underlying units (S or T). Surface discolouration varies from pale calcrete through grey to black (Munsell N8/0 to N4/2).

The entire stone assemblage occurs with a thin matrix of reddish-brown sand, the basal facies of the overlying unit Q sand. The main fire evidence is found on the headland platform, a relatively small area 2–4 m wide by 45 m long east–west at the foot of cliffed unit Q sand (Figure 9). Occasional gravel-sized stones have also been recovered from higher in the Q sand.

Lithological changes

Variations in darkening are reflected in acid insoluble residues of the dominantly Rcp calcrete parent. By thin-section inspection, Rcp has the following components:

- sand-sized marine shell fragments, 40–50%
- 0.2–0.4 mm quartz sand, 15–20%
- micritic calcite cement, 25–30%.

Acid dissolution of pale calcrete yields a quartz sand residue in a clear supernatant liquid. By contrast, darkened samples yield similar quartz in very dark grey–brown cloudy liquid, a reflection of significant mineral change associated with the darkening process.

Across both West Stack and the headland, detailed field observations reveal an inverse relationship among the intensity of darkening, stone size and degree of rounding. As presented diagrammatically (Figure 12), larger angular blocks are only lightly darkened (N7/0 to N6/0) and usually on one side only. Smaller rounded stones are more uniformly affected (all surfaces), with high-intensity

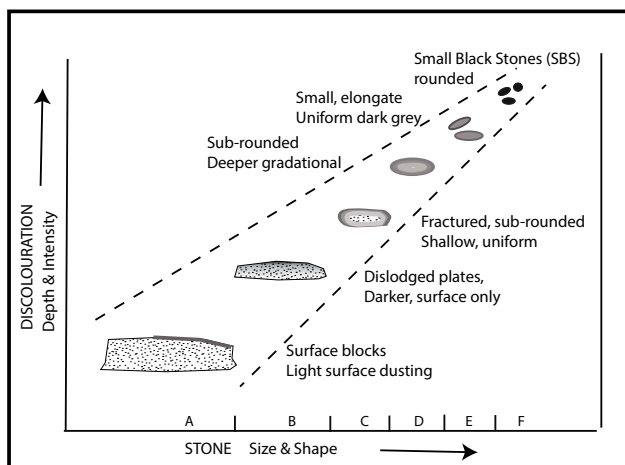


Figure 12: Classification of stones (A to F) based on size, shape (rounding) and depth of discolouration. The categories reflect cumulative effects, potentially of fire.

colours to nearly black (N5/0 to N3/0). Importantly, the depth of discolouration varies from negligible in larger angular blocks to pervasive in many small, more rounded specimens.

Fractures and darkening. Where stones have been subjected to secondary fracturing, the retention of sharp edges implies their preservation by rapid burial. For example, a large (25–30 cm) calcrete block (Figure 13) fractured *in situ* and weakly cemented onto G α on the headland, displays surficial dark grey patches but has an unaltered pale core. The block has been shattered with a radial fracture pattern consistent with thermal expansion (Bowling et al. 2016). Additional evidence suggestive of heating is provided by the marginal surface darkening. The jigsaw fit of the block's fragments indicates long-term stability since fracturing.

A second fractured stone embedded in unit Q sand above G α on the headland features colour zonation, where the darkening diminishes in intensity from dark grey on one surface to unpigmented at about 2 cm below the surface (Figure 14).

West Stack–headland contrasts. On the headland, traces of charcoal dispersed in unit Q sand (Nair & Sherwood 2007) provide evidence of sporadic fire during aeolianite accumulation. On West Stack, darkened stones, associated shells and pinkish sandy matrix were transported as a debris flow, triggered by the Z-event. No other shell accumulation or post-transport darkening appears to be present. By contrast, on the headland, the darkened stones exist as two populations. The first consists of stones embedded in or mantled by the pinkish matrix of the mass-flow deposit, as on West Stack and Block Dii (Figure 10B). The second involves stones supported by sand lying above and free of the pinkish matrix. That the darkening process continued on the headland after the Z-event is corroborated by the presence there of a possible fireplace lying undisturbed in overlying unit Q sand (Figure 15).

Place of fire: Fp1

While traces of charcoal in unit Q (Nair & Sherwood 2007) represent sporadic evidence of fire, the fire study began in earnest with the discovery (28 February 2007) of traces of charcoal in basal Q sand resting disconformably on G α (Figure 15B). Designated here as 'a place of fire', Fp1, the validity of the human connotation of 'fireplace' remains to be established.

Near the western margin of the headland, a group of stones with fragments of charcoal provided the first links between the pattern of darkening and fire. A lens of dark brown, humic sand, about 15 cm thick and 80–120 cm across, was exposed by excavation within brownish sand at the base of unit Q. Further excavation revealed a number



Figure 13: Large (20–25 cm) stained calcrete block on headland Gsa. Radial fractures associated with darkened circumference provide evidence of thermal expansion. Knife blade is 20 cm.

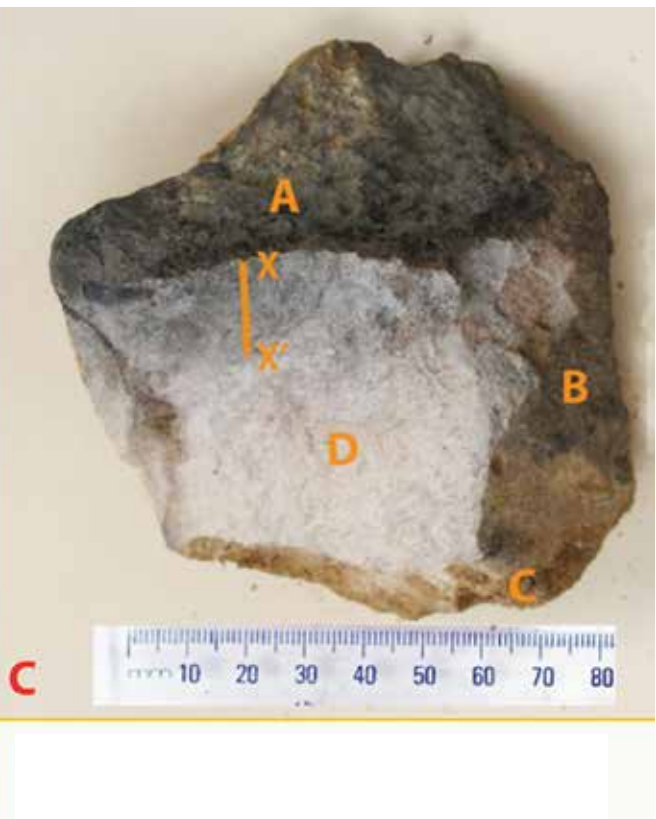


Figure 14: Burnt *in situ* stone.

LEFT: A. Stone of broken calcrete with dark surface lying on headland Gsa. B. Stone removed to show staining zonal effects.

RIGHT: Alteration sequence on stone's faces reflect sequence of events.

A. Irregularly fractured surface from formerly planar calcrete, now blackened.

B. Surface remained unaffected by blackening process.

C. Thin coating of red calcareous sand cemented to surface B.

D. Fresh fracture showing zonal surface staining grading to pale calcrete below.

X-X'. External zone, ~2 cm thick, showing gradation from blackened upper surface to unaffected calcrete. Orientation reflects high temperature on horizontally undisturbed platform surface.

of confirmatory features (Figures 15C, D). A centrally located rectangular calcrete block approximately 25 x 15 cm occurs in a depression in the underlying calcrete surface (Figure 15D). Lying on, and weakly cemented to, the surface of the block, is an angular fragment, ~5 x 5 cm, of pinkish limestone with a small fragment of the same

lithology alongside (Figure 18A). The singular occurrence of two limestone fragments perched and cemented in place on an isolated calcrete block is difficult to explain by any natural depositional process.

Around the central block, the depression in the basal calcrete was filled with a mixed assemblage of small

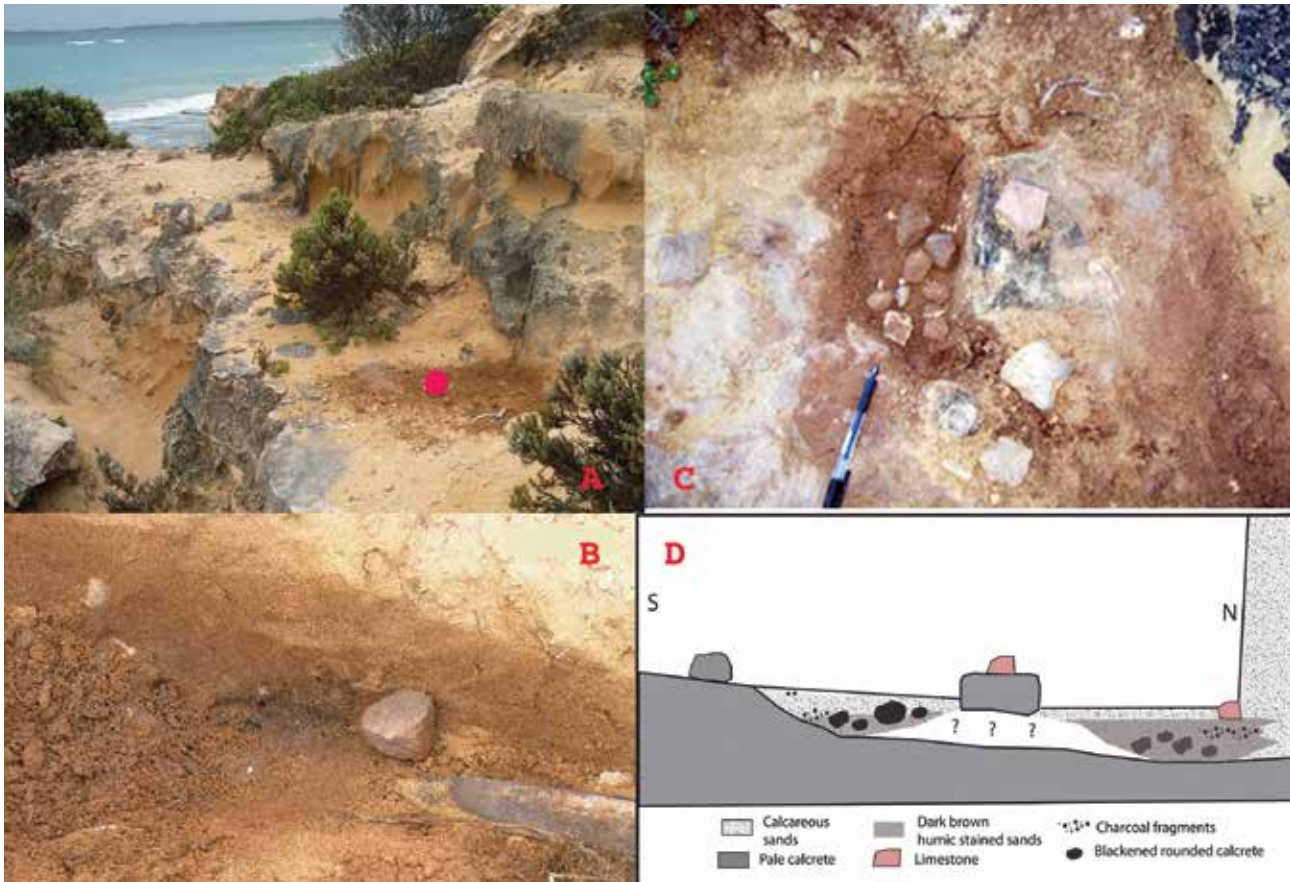


Figure 15: A. View west across headland bench (G_{sa} , Figure 9) below calcrete on unit Q sands showing location of a possible fireplace (Fp1) in dark brown zone at base of small cliff cut into unit Q.

B. Dark brown lenticular zone with charcoal fragments at base of unit Q sands in Fp1. Knife blade 2.5 cm wide. Note cobble of red limestone with darkened interior against cliff wall.

C. Vertical view of fire affected area surrounding a central calcrete block. Charcoal zone lies at base of right cliff wall.

D. Diagrammatic north-south cross-section through Fp1. Irregular depressions containing small black stones are separated by larger calcrete block carrying small red limestone atop central block and at base of wall in B. Clusters of small black stones in depressions on either side of the central block. See Figure 18.

blackened stones together with occasional less blackened, rounded or angular fragments of paler calcrete (Figures 15C, D) with distinctive small fragments of charcoal (Figure 15A). Evidence of a fire horizon, when traced horizontally into the lowest level of the vertical face, is continuous with a lens of similar very dark brown sand and a central concentration of charcoal fragments (Figure 15B). This site was subsequently excavated to reveal additional features consistent with the possibility of a hearth (McNiven et al. 2018). In summary, the following characteristics are present:

1. A clustered arrangement of stones (calcrete and calcarenite) with varying degrees of darkening
2. A near-circular horizontal zone of humic-darkened sand on both sides of a central calcrete block
3. A lenticular zone of charcoal-associated, humic-darkened sand
4. Charcoal fragments in association with blackened, apparently heat-affected stones.

The evidence is consistent with the features being a substantial ‘place of fire’, but can it be described as a ‘fireplace’ with the human connotation of that term?

Second place of fire: Fp2

In late 2016, a second ‘place of fire’ (Fp2), was located approximately 10 m east of East Point on the headland (Figure 2). Unit Q here is thin, about ~1 m thick, and is capped by calcrete Qcs. The hearth-like feature is >1 m in north-south exposure (Figure 16). It lies within LIG unit Q (Sherwood et al. 2018b) on a narrow erosional bench ~30 cm above G_{sa} and ~40 cm below unit Q calcrete (Qcs, Figure 17). The feature’s assemblage of transported calcrete stones includes reddish (pedogenic) calcrete, pale calcrete blocks ≤ 10 cm with darkening, and small golf-ball-sized blackened stones. Several calcrete blocks, 10–20 cm in diameter and buried in the aeolian sand of unit Q, probably derive from calcrete of unit R (Rcp or Rcs). A number of small black stones closely resemble



Figure 16: A. Fp2 suspected fire site, vertical view, near-circular group of stained stones with concentration of small black stones associated with strong reddish-brown sands of unit Q. Inset B. Dark-stained calcrete stones lying under calcrete overhang. Inset photograph: J. Sherwood.

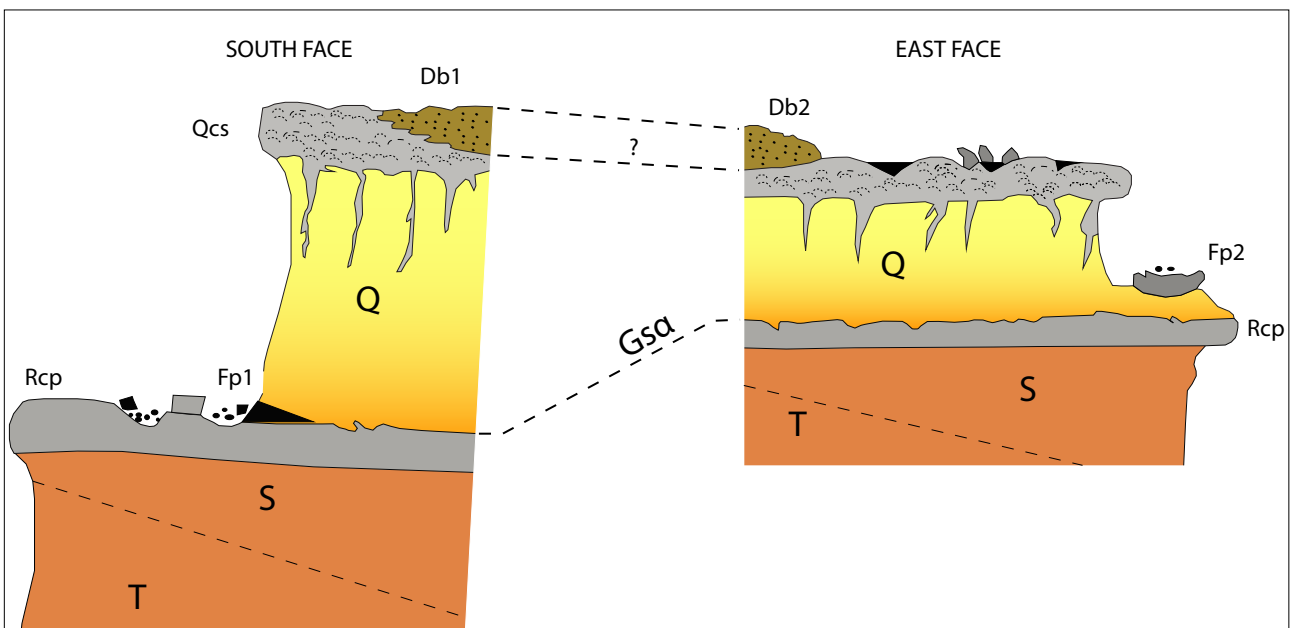


Figure 17: Stratigraphic correlation between Fp1 cliffed features on South Face (Figure 2) and Fp2 exposures in equivalent last interglacial Unit Q sands on East Face (Figure 2). Detailed evaluation of Fp2 awaits further work. Artwork: Jeremy Ash.

those excavated from the basal zone of Fp1 (Figure 15D). Some large transported blocks of calcrete lying in close juxtaposition exhibit strong surficial grey darkening typical of those on Gsa (South Face) inferred to be fire-affected. The arrangement of stones, their blackening and the necessity for their transport by a mechanism other than wind point convincingly to Fp2 as a specific location of fire.

The fire-darkening hypothesis gains credence from the charcoal evidence of Fp1, whose blackened stones are similar to those of Fp2 (Figures 15D, 18B) and occur at essentially the same stratigraphic level in different places representing similar ages.

EXPERIMENTAL HEATING

Testing in fire

Can the stone darkening of both the headland and West Stack be shown to be a legacy of fire? Experimental evidence helps answer that question.

The inverse association between intensity of darkening and stone size (Figure 12) suggests a causal relationship. Charcoal associated with Fp1 indicates at least some occasions of burning. To test the effects of heating on calcrete, four white angular fragments of calcrete Rcp were placed in a small wood fire for one hour. The fragments showed a progressive change from light grey to darker grey and eventually near-black. After 60 minutes (Figure 18) the colour of both the surface and the interior had turned to near-black. Exfoliation had resulted in smaller particle size and a lessening of angularity. In some fragments, the outer



Figure 18: Experimental fire conversion to dark calcrete.

- A. Two small fragmented components of pinkish limestone (unit S) balanced on top of central calcrete block in zone of fire-affected area, Fp1. See Figure 15, C and D.
- B. Small black stones excavated either side of central calcrete block, Fp1, as in Figure 15, C and D. Small thoroughly blackened stones from depression at possible fireplace (Fp1, Figure 15). Coin is 29 mm in diameter.
- C. White calcrete fragments (Rcp) selected for heat treatment in wood fire.
- D. Same stones after 40–60 minutes in wood fire, thoroughly blackened with rim traces of white calcined lime reflecting temperatures $>700^{\circ}\text{C}$. Note similarity with stones from fire excavation in B above.

parts turned a creamy white, reflecting reduction to lime by loss of carbon dioxide at high temperature ($>730^{\circ}\text{C}$; Gonzales-Gomez et al. 2015; Moropoulou et al. 2001).

This small experiment supports the following conclusions:

1. Initially the outer surface close to the coals is discoloured while the inner core remains unchanged.
2. Complete inner blackening needs the most time. It requires close proximity to coals and a long period of gradually increasing heat.
3. Conversion of calcrete from pale to grey to dark grey and then to near-black requires heating to high temperature and for a relatively long time (up to one hour), an observation consistent with earlier work (Shinn & Lidz 1988).
4. Some exfoliation occurs, with diminution in size as well as rounding as the calcrete turns black.

The experimental evidence supports the contention that blackened stones from the headland, as in Fp1 (Figures 15, 18), were situated around a centrally located heat source and subjected to high temperature for a long time. Such features are consistent with development in a structured hearth. The evidence from this single experiment requires corroboration from multiple darkened examples. Magnetic susceptibility offers that possibility.

MAGNETIC SUSCEPTIBILITY

Changes in iron mineralogy involving production of magnetic minerals, such as magnetite and maghemite, as a result of heating have long been known (Peters & Thompson 1999; González-Gomez et al. 2015). Enhanced magnetic susceptibility (MS) has been found in studies of archaeological sites (Gedye et al. 2000; Herries 2006; Herries & Fisher 2010) and of heat-affected soils (Oldfield

& Crowther 2007; Mullins 1977). A susceptibility survey was undertaken to determine if stone darkening was accompanied by increased MS and, thus, likely to be thermally induced.

Field methods

A Bartington Susceptibility Meter with MS2 sensor (25.4 mm diameter response) was used to survey discoloured stones across Gs α on the headland. MS is reported in SI units ($10^{-8}\text{ m}^3/\text{kg}$). Some 70 samples were measured across the range of surface variation from pale calcrete to darkened examples. MS results represent integrated values within the 25.4 mm sensor's cone of measurement. The relationship among stone size, shape and intensity of discolouration was recorded photographically (Figures 19–21).

Results

A strong association is determined between MS and the intensity of darkening in specimens ranging from unaltered calcrete blocks through to nearly black small stones. Large rectangular blocks of calcrete with only minor superficial darkening have low to zero susceptibility. Measurements above about 5 SI almost always display a significant degree of darkening. Where carbonate blocks are only partially darkened, as in the case of the radially fractured block (Figure 13), the MS signal is small (1–3 SI). When considered with respect to unit volume, the susceptibility signal of thin surficial blackening is dwarfed by the near-zero value of the large volume of relatively unaffected calcrete coming within the sensor's range. The results from such samples are uniformly low. Results are also colour sensitive. Only strongly blackened samples (Munsell range N4/0 to N2/0) provide MS values in the 40–71 SI range.



Figure 19: A. Cluster of stones on Gs α of Point Ritchie headland showing range of magnetic susceptibility (MS, in red) associated with colour variation. MS values range from 1 to 71 SI with higher values in more intensely darkened stone. Yellow ellipse shows approximate area of B.

B. Stone 1, small black stone (170513/1) with highest susceptibility (71 SI), selected for TL analysis (W4697), provided ages of 109 ± 8 ka and 93.2 ± 7.2 ka. Note adjacent clustering of small black stones, rounded and set in red-brown sands, suggesting resemblance to a collapsed hearth.



Figure 20: A. Scatter of calcrete stones on headland Gsa exhibiting a range of susceptibility readings (in red) of 5 to 41 SI, with pale calcrete consistently below 10 SI, in contrast to darker blocks (18–41 SI). Yellow square approximate area of B. B. Stone 2 location (170513/2, Table 2) (MS = 41SI), used for TL analyses (sample W4698) giving ages shown.

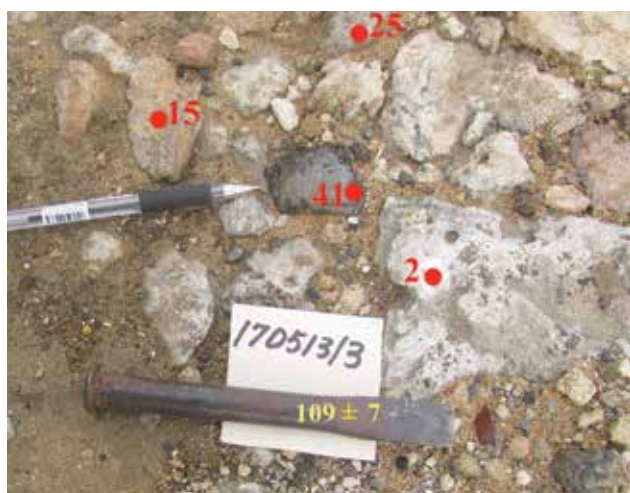


Figure 21: Stone 3 — Range of pale to reddish calcretes in assemblage of black, rounded stones, susceptibility range 2–41 SI from pale to black. Reddish stone on left, MS 15 SI, probably reflecting ferric iron content. Note smooth abraded calcrete (MS 2 SI) with possible vertical pholad hole. Entire assemblage set in red-brown sand. Location of stone 170513/3 (MS = 41 SI), used for TL dating (sample 4699) with age 109 ± 7 ka.

Blocks with dark-grey zonation provide variable readings in the range ~15–35 SI. The only values greater than 35 are preserved by small and very dark (nearly black) samples, e.g. the TL samples of three stones 1, 2 and 3 (71, 41 and 41 SI, Figures 19–21 respectively). In summary, the correlation between small dark samples and high MS values reflects a change consistent with progressive heating.

Several factors complicate interpretation of the MS data. While a general relation exists between particle size and the intensity of darkening on one hand and MS on the other, this relation breaks down in the presence of ferric-rich matrix. Thus:

1. Measurements were limited to calcrete with pale to black darkening. Samples of reddish limestone which have high MS values were excluded on the basis that it was not possible to discriminate between the susceptibility effects of heating and lithology.
2. While pale calcrete yields uniformly low values (0–5 SI), the presence of red pigmentation without any evidence of thermal discolouration typically results in MS values in the range 5–15 SI, a result attributed to coating by Z-event, ferric-rich matrix.

The samples illustrated (Figures 19–21) are representative of both the range of variation in MS values and the degree of alteration of the original calcrete blocks. They include samples used in TL analysis. It is appropriate here to consider the significance of one distinctive group of darkened rocks, the small black stones (SBS). They represent an end member of the shape–darkening classification (Figure 12). They yield the highest MS values of the entire stone population. Clustering of small black stones is consistent with darkening due to heating in small, localised fires followed by slight disturbance with scattering.

The occurrence of charcoal in Fp1 with SBS confirms the latter's association with fire (Figure 15). Consistent with the prediction of magnetic minerals as a result of heating (Peters & Thompson 1999; González-Gomez et al. 2015) the insoluble residue from the highest MS sample, W4697 (Figure 19, Table 2), contained black magnetic platelets, a feature consistent with the otherwise dark grey amorphous residue described earlier. X-ray diffraction analyses of two residual samples W4697 and W4698 (Stone 1 and Stone 2 respectively, Table 2) record maghemite as a predicted thermal product. Calcrete darkening is now confirmed as the result of fires. The ages of those heating events remain now to be identified.

TL AGES

While the stratigraphic envelope of the darkened stones is shown to be LIG, the timing of actual fires is another matter. The temperatures required to transform calcrete from pale grey to near-black in the experimental fire, estimated in excess of 350–500°C (i.e. those of red-hot coals), would thermally reset quartz luminescence signals and potentially record the age of heating (Aitken 1998). TL analysis of SBS provides a test for that possibility.

Methods

Three small blackened calcrete stones with high MS values (71, 41 and 41 SI, stones 1, 2 and 3 respectively) were selected from Gsa for analysis (Figures 19–21). Pieces of stones 1 and 2 (W4697 and W4698, Table 2, Figures 19–20) were initially cleaned to remove any adhering sediment before immersion in a HCl acid bath to dissolve CaCO₃ and thus recover any granular insoluble residue. For both stones this cleaning step was repeated on replicate pieces. For sample numbers with suffix A, care was taken to remove even more of the surrounding sample crust to ensure no surficial soil remained prior to acid dissolution.

Following neutralisation, the 90–150 µm quartz grain-size fraction was separated by wet sieving, etched in 40% HF and subjected to heavy liquid separation. Using a volumetric method, twenty sample aliquots were deposited onto aluminium planchets. Six of these were used to determine the natural TL acquired since their last resetting and the remaining fourteen were incrementally irradiated in pairs using a calibrated ⁹⁰Sr-plated plaque radiation source. These were used for the preparation of a TL growth curve from which the equivalent radiation dose was determined.

A third stone (sample W4699) was considerably smaller than stones W4697 and W4698 and therefore the grain-size fraction analysed was expanded to 90–180 µm. Nevertheless, sufficient sample for only five aliquots was obtained. This was HF-etched but not subjected to heavy

liquid separation because of concern for sample loss during the process. A single aliquot was used for the measurement of the natural TL signal and four in the preparation of the TL growth curve.

Each of the sample aliquots was placed in a TL glow oven and heated to 500°C at a rate of 5°C/second in a high-purity nitrogen atmosphere. The TL signal emitted was recorded using an EMI 9635QA photomultiplier fitted with suitable light and heat filters. In order to correct for disc-to-disc variation, all output signals were normalised by means of a second glow procedure following a standard laboratory irradiation. From the data obtained, an additive TL growth curve was prepared from which the equivalent radiation dose acquired was determined.

The internal radiation dose was measured by means of thick-source alpha counting (TSAC) over a 42-mm scintillation screen to determine the (U + Th) activity. K concentration was evaluated by atomic absorption. Radiation dose rate included corrections made for the external environmental dose-rate measurements made on burial-context sand using TSAC and atomic absorption.

Burial depth was assumed to be 2.8 m for calculation of the cosmic radiation contribution to dose, and moisture content was assumed to be 7.5% (the mean of various moisture determinations in unit Q sand). Rubidium content was assumed to be 25 ± 10 ppm. This makes only a minor contribution to the overall radiation dose.

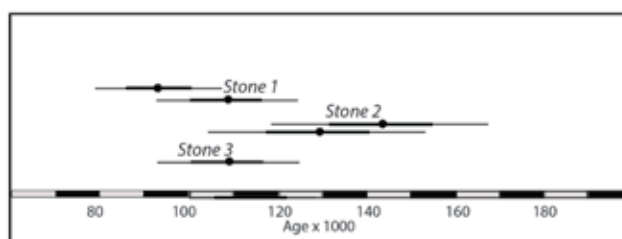


Figure 22: TL ages of black, suspected hearth stones with luminescent signatures reset by heating: Three black stones (1 to 3) from Headland Gsa dated by Price (this paper). Ages at both 1σ and 2σ. See text for comments.

Table 2: Data for TL age determination of three black stones from Gsa. Age uncertainties are 1σ. Samples W4697A and W4698A from inner parts of stone.

Sample / Stone	K (%)	Rb* (ppm)	Sp. activity (Bq/kg)	Water* (%)	Cosmic dose (Gy/ka)	Total dose rate (Gy/ka)	ED (Gy)	Age (ka)
W4697 1	0.12	25	18.1	7.5	0.14	0.657±0.022	71.8±5	109±8
W4697A 1	0.12	25	18.1	7.5	0.14	0.657±0.022	61.2±4.3	93±7
W4698 2	0.125	25	17.8	7.5	0.14	0.674±0.023	86.8±7.8	129±12
W4698A 2	0.125	25	17.8	7.5	0.14	0.674±0.023	96.3±8.7	143±14
W4699 3	0.085	25	14.7	7.5	0.14	0.613±0.030	67±3.2	109±7

* Assumed values.

Results

Results of the TL study are summarised in Table 2 and Figure 22. Replicate analyses of samples W4697 and W4698 are in agreement with age estimates overlapping at the 2σ level (W4697 = 101 ± 11 ka; W4698 = 136 ± 18 ka). All three stones give ages in the LIG range (101–136 ka), with two stones (W4697, W4699) having similar ages, possibly younger than W4698 (Table 2).

These results were derived from SBS samples, blackened throughout. A complication arises in cases of partial blackening which, if due to fire, implies a thermal gradient from a stone's outer surface to its unaffected core. This suggests variation in the TL signal of the stone from thermal control on the surface across the internal threshold to unaltered or unaffected toward the core. Only the small black stones are likely to have experienced uniform resetting of TL.

DISCUSSION

The association of darkened stones with midden shells on West Stack (Sherwood et al. 2018a) and their frequency across headland outcrops establishes these as features centrally important to the site's significance. While evidence of fire has been established, especially for SBS examples, does it account for the entire range of stone darkening?

Cause of darkening

Many factors may contribute to the process of darker colouration. The explanation must account for the following characteristics:

1. Stain versus shape correlation. Only the smallest stones (SBS) are pervasively blackened. Larger calcrete blocks display only limited thin darkened zones. The SBS end member of the shape-darkening gradient (Figure 12) reflects a genetic process that extended both through time and in space across West Stack, the headland and Block B.
2. Zonal colour variation from the surface to the stone's core and, in SBS, blackened throughout.
3. The SBS-charcoal association at Fp1 (Figure 15), which suggests a causal relationship between *in situ* fire and calcrete darkening.
4. Strong correlation of MS with darkening intensity, which reflects a range in degree of thermal alteration in stone populations, from large, weakly darkened, low-MS clasts to the SBS group with the highest MS values. The presence of a magnetic mineral residue in two samples after treatment for TL analyses is consistent with established effects of heat on limestone (Oldfield & Crowther 2007; Mullins 1977).

5. Effects reproduced experimentally (Figure 18), which resemble those uncovered in Fp1. Darkening required exposure to high temperatures for nearly one hour.

Although many factors may produce surface effects, e.g. manganese or biofilm stains, deep penetration here rules out such surface effects. Conversely the mineralogically controlled blackening here, exemplified by iron transformation from soluble to insoluble residues, a ferrous to ferric transformation (evident as XRD-determined maghemite, formed by fire), is quite unlike South Australian biogenic examples (Miller et al. 2013). Additionally, the absence of soils on both West Stack and the headland platform excludes a pedogenic influence. Fire remains the most likely cause of the wide variety of darkened stones. One additional line of evidence is important.

The fire experiment reveals another important consideration. Requirements to produce transformation to black, high susceptibility (magnetite, maghemite) include high temperature and long duration. These are precisely those required for calcining (Moropoulou et al. 2001). As reproduced experimentally (Figure 18D), these temperatures are first reached on outer stone margins. After a single event in the field, any rim of soluble white lime (calcium oxide) is removed in the next wet season.

Recurrent firing would produce size reduction with progressive removal of surface irregularities involving progressively increased rounding. The recorded pattern of size, staining and rounding (Figure 12) is entirely consistent with progressive firing to produce the SBS end products in observed stone records. In summary, field records and experimental evidence are in agreement. The small black stones developed by repetitive firing resulting in progressive reduction in size and change of shape.

Their occurrence on Gs α over the entire headland from south- to east-facing parts implies the repeated existence of small localised fires across a confined surface adjacent to coastal cliffs. Although SBS are dispersed across Gs α , their occasional clustering (Figures 19, 20) suggests their derivation from disturbed hearth-like structures such as Fp1 and Fp2.

Age of fires

Three independent lines provide evidence of now-secure age dating.

- On the headland, examples Fp1 and Fp2 lie either in or beneath a cover of unit Q aeolianites dated at 120–125 ka (Sherwood et al. 2018b).
- Blackening on the abrasion platform of Block B post-dates marine retreat from the maximum +8 m AHD 125 ka sea level.
- Direct TL dating of thermal resetting with results in

the range 100–140 ka confirms ages within the LIG.

The magnitude of exposure to heat, evidenced by hundreds of examples of SBS at Moyjil, now requires explanation.

Wildfire as possible cause

With fire-affected stones scattered over the entire $G_{s\alpha}$ exposure, could the explanation lie with natural, episodic wildfires? The following points are relevant:

1. Darkening intensity is not random. The relationship between increased MS on one hand, and decrease in stone size and increased depth of blackening on the other (Figure 12), is unlikely in a natural fire regime. This inverse correlation suggests an element of selection in the firing process.
2. The production of the population of SBS requires high temperatures around 800°C over an extended period.
3. Fractured stones commonly show at least two generations of fracturing (Figures 14, 18A).
4. The lenticular pattern of charcoal concentration in humic sands overlying fire-blackened stones in the Fp1 depression (Figure 15) suggests repetitive fire at the same place.
5. The erosional surface, $G_{s\alpha}$, cutting across fractured Rcp calcrete and the palaeosol of unit S (Figure 11) lacks any traces of vegetative cover. Unit Qcp rhizomorph traces on block B (Figure 11) overlie the blackened region demonstrating the later presence of plants sustained by sediment cover after, but not before, heating. The implied absence of onsite fuel on bare rock surfaces renders unlikely a natural fire agency. If fire be the cause, it required importing fuel by an independent agent.
6. The clustered distribution of many SBS is consistent with their association with separate fires but inconsistent with the more generalised effects of wildfire.
7. The contrast between strong pervasive discolouration of the SBS and only surficial darkening of larger blocks points to a separate and specific history of the SBS group. These most strongly fire-affected stones, the dominant SBS group, occur over the entire platform suggesting repetitive events producing similar end products over an extensive region.

Possible hearths

Although any definitive hearth structure remains elusive, the following observations are pertinent.

1. The structure of Fp1 with balanced and blackened stones in a basal pit overlain by charcoal retaining sand bears at least superficial resemblance to a

hearth. Excavation (McNiven et al. 2018) admits the possibility of Fp1 as a degraded hearth.

2. The construction of Fp2 involved movement of stones from the underlying calcrete. Variable blackening of stones included the production of residual SBS. As a result, Fp2 bears a resemblance to Fp1 (Figures 16, 17).
3. While broadly scattered, the tendency of SBS to occur in clusters is consistent with degradation from an originally more ordered distribution. Erosional deflation of a feature like Fp2 would be capable of reproducing such clustering of SBS.

The evidence is consistent with stones being collected at particular points on $G_{s\alpha}$ and heated in a situation reminiscent of a hearth. If subjected to disturbance by the Z-event, as on West Stack, or burial by unit Q sand, consequent hearth collapse would be consistent with the observed scatter of hearth-derived SBS over the entire area of the proposed occupation surface. Despite a two-year embargo on its study (Fp2, due to absence of any permit), one of us (JMB) believes this site already demonstrates close identity to a degraded hearth. Its detailed evaluation is awaited as the closing chapter of a full fire-environment story.

In summary, although no single line of evidence precludes natural fire, taken collectively the case for exclusion is strong. Humans are obviously capable of these processes, of carrying fuel to a cliffed shoreline and repetitive burning at the same place.

On the basis of present evidence, human agency is a viable explanation. The prospect, however, of humans in that locality at 120 ka, although consistent with evidence, presents more questions than answers. Who were they? Why here and not elsewhere? Why no legacy of any toolkit, no traces of food let alone human remains?

In the absence of bones, stone flakes or any independent trace of people, the notion of occupation at 120 ka currently remains difficult to credit. However, marine shells, stones in unexplained depositional context and fire resemblance to hearth, successively diminish the possibility of a natural explanation. That absence leaves the currently unlikely option of human agency as the most likely alternative.

Environmental summary

Dated geomorphic features at Moyjil permit the establishment of the historical relationships between sea level, interpreted seismic disturbance (Z-event) and fires. The Z-event and burning occurred on this coastal margin during the LIG as sea level fell from +8 m to +6 m AHD and before deposition of unit Q aeolianite. Summarised in Table 3 and Figure 23, it highlights the ‘snapshot’ nature of this report’s main focus, the LIG (120–125 ka, MIS

5e). Some 50,000 years before the currently accepted time of human arrivals (Clarkson et al. 2017; O’Connell et al. 2018), the brief record of fire without trace of flaked stone or bone stands as a solitary instance posing more questions than answers.

CONCLUSION

At Moyjil, the effects of fire are identified in close association with the erosional surface (Gsa) and the basal sand of unit Q. Such effects include charcoal, variable blackening of calcareous stones and the variation in magnetic susceptibility of stones. The field evidence

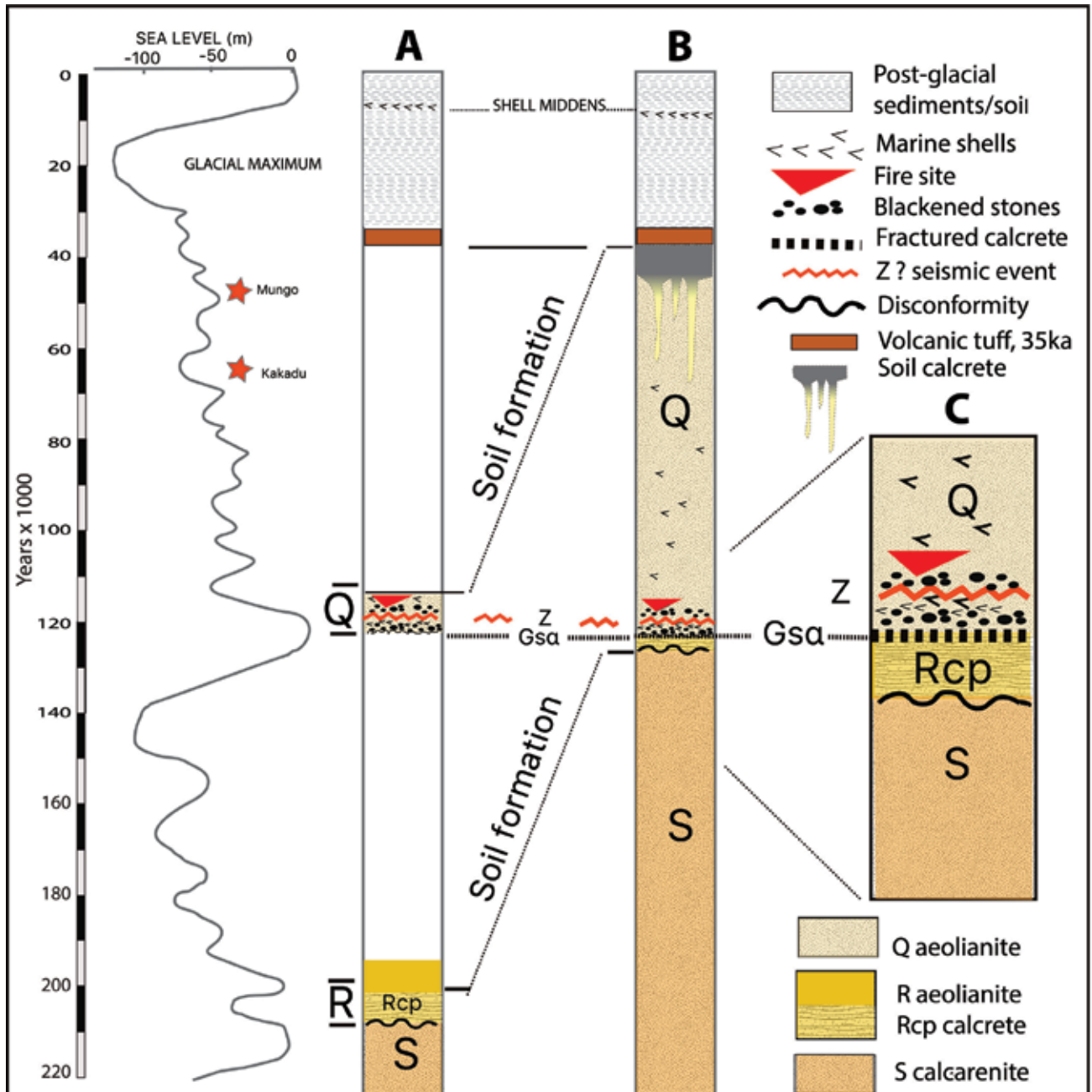


Figure 23: Diagrammatic relationships between fired stones, shells and time-related environments. Three columns relate stratigraphic and geomorphic features to changing sea level over the past 200,000 years.
 A. Litho-stratigraphic illustration of sediment–soil relationships, units as per Table 1. Episodic interglacial high sea level controlled aeolianite deposition of successive units S, R and Q to the present post-glacial. (SL data from Chappell et al. 1996; Railsback et al. 2015.)
 B. Exposure details in this study presented as lithologic units. Features of interest are constrained by the short time interval of fire and shell occurrences, about 10,000 years within the timeframe of 200,000 years.
 C. Enlargement of special interest features, shells with fire affected stones on Gsa erosion surface. Seismic interruptions during time of fires pre-dating main unit Q deposition, with continuation of occasional shell collection.
 Red stars, ages of two archaeological sites relative to potential occupation suggested here by fires. (Mungo, Bowler et al. 2012; Kakadu, Clarkson et al. 2017).

of darkened stones, supplemented by the experimental burning of calcrete, is now explained as the legacy of fire. Consistent with independent stratigraphic and OSL ages, thermoluminescence results confirm ages during MIS 5e (~120–125 ka), before deposition of associated unit Q aeolianites. In the absence of any evidence of natural fire, the suggestion of possible hearths points somewhat uncomfortably towards human agency. For some, an acceptance of human presence in Australia 120,000 years ago as a *possibility* may now tentatively advance to one of

probability. For most, the question of Australia’s occupation at that time remains highly contentious. Different people will attach different levels of significance to the various lines of evidence presented here.

Evaluation of site Fp2 is eagerly awaited. In the meantime, despite the lack of conclusive evidence, the pendulum in the Nature–People controversy has swung in one direction. The mere suggestion of people near 120 ka raises an entirely new set of questions in the exploration of Australia’s human story.

Table 3: Sequential record of environmental change associated with evidence of fire-related events in estimated time scale

Age ka	Environmental history
~300	Deposition and soil on reddish calcarenite, unit S
~200	SL rise, truncating unit S, aeolianite deposition, unit R
200–125	Fall in SL, soil formation and deep groundwater calcrete Rcp on permeability barrier over S
125–120	Interglacial SL rise to +8 m abrasion on repositioned block B, erosional development new Ground surface Gsa, cut across unit R calcrete
120	Slight drop in SL, fires on abrasion surface block B, shell collection & stained stone deposition on West Stack Major (?) seismic disturbance, Z-event, fracturing calcrete on Gsa, fluid mobilisation of shells and stones, West Stack Collapse of stack-headland connection, deposition of boulder talus with formation of cobble beach at +6m SL
115–110	Early fall in SL, deposition unit Q aeolianite with occasional shell and fire. 103 ka calcite infill of Z fractures
110–40	Low SL, soil formation on unit Q, development of calcrete Qcs
40–25	35 ka deposition Tower Hill ash, local erosion, Ground surface Gsβ with hearths (Carey et al. 2018)
25–15	Glacial maximum, lowest SL
15–0	Post-glacial SL rise to present, exhumes palaeotopography

Acknowledgements

Primary field data and this report by JMB, TL analyses by DMP, co-authorship (JES & SPC) in acknowledgment of joint collaboration. Research in collaboration with Eastern Maar Aboriginal Corporation, Gunditj Mirring Traditional Owners Aboriginal Corporation and Kuuyang Maar Aboriginal Corporation. Stafford McKnight, Federation University Australia, provided XRD analyses. Dr Jeremy Ash, Monash University, generously drafted Fp2 diagram (Figure 17). Jessica Reeves, John Webb and Mark Quigley commented in the field. JMB thanks Cliff Ollier, Andy Herries and Frank Oldfield for comments on early drafts. Two referees are thanked for their insightful and constructive comments. Awaiting further investigation of the 2016 discovery of Fp2, this paper was structured as a Bowler-Price interim report to the field management group.

References

- Aitken, M.J., 1998. *Introduction to Optical Dating: The Dating of Quaternary Sediments by the Use of Photon-stimulated Luminescence*. Clarendon Press, 280 pp.
- Bowler, J.M., Gillespie, R., Johnston, H. & Boljkovac, K., 2012. Wind v water: glacial maximum records from the Willandra Lakes. In *Peopled Landscapes: Archaeological and Biogeographic Approaches to Landscapes*, S.G. Haberle, & B. David, eds. *Terra Australis* 34: 271–296.
- Bowning, J., Meredith, P. & Gudmundsson A., 2016. Cooling-dominated cracking in thermally stressed volcanic rocks. *Geophysical Research Letters* 43: 8417–8425.
- Brooke, B., 2001. The distribution of carbonate eolianite. *Earth Science Reviews* 55: 135–164.
- Carey, S.P., Sherwood, J.E., Kay, M., McNiven, I.J. & Bowler, J.M., 2018. The Moyjil site, south-west Victoria, Australia: stratigraphic and geomorphological context. *Proceedings of the Royal Society of Victoria*, this volume.
- Chappell, J., Omura, A., Esat, T., McCulloch, M., Pandolfi, J., Ota, Y. & Pillans, B., 1996. Reconciliation of late Quaternary sea levels derived from coral terraces at Huon Peninsula with deep sea oxygen isotope records. *Earth and Planetary Science Letters* 141: 227–236.
- Clarkson, C., Jacobs, Z., Marwick, B., Fullagar, R., Wallis, L., Smith, M., Roberts, R.G., Hayes, E., Lowe, K., Carah, X., Florin, S.A., McNeil, J., Cox, D., Arnold, L.J., Hua, Q., Huntley, J., Brand, H.E.A., Manne, T., Fairbairn, A., Shulmeister, J., Lyle, L., Salinas, M., Page, M., Connell, K., Park, G., Norman, K., Murphy, T. & Pardoe, C., 2017. Human occupation of northern Australia by 65,000 years ago. *Nature* 547: 306–310.
- Gedye, S. J., Jones, R.T., Tinner, W., Ammann, B. & Oldfield F., 2000. The use of mineral magnetism in the reconstruction of fire history: a case study from Lago di Origlio, Swiss Alps. *Palaeogeography, Palaeoclimatology, Palaeoecology* 164: 101–110.
- González-Gómez, W.S., Quintana, P., May-Pat, A., Avilés, F., May-Crespo, J. & Alvarado-Gil, J.J., 2015. Thermal effects on the physical properties of limestones from the Yucatan Peninsula. *International Journal of Rock Mechanics & Mining Sciences* 75: 182–189.
- Hearty, P.J., Hollin, J.T., Neumann, A.C., O’Leary, M.J. & McCulloch, M., 2007. Global sea-level fluctuations during the Last Interglacial (MIS 5e). *Quaternary Science Reviews* 26: 2090–2112.
- Herries, A.I. R., 2006. Archaeomagnetic evidence for climate change at Sibudu Cave. *Southern African Humanities* 18(1): 131–47.
- Herries, A.I. R. & Fisher, E.C., 2010. GIS modeling of magnetic mineralogy as a proxy for fire use and spatial patterning: Evidence from the Middle Stone Age bearing sea cave of Pinnacle Point 13B (Western Cape, South Africa). *Journal of Human Evolution* 59: 306–320.
- McNiven, I.J., Crouch, J., Bowler, J., Sherwood, J., Dolby, N., Dunn, J.E. & Stanisic, J., 2018. The Moyjil site, southwest Victoria, Australia: excavation of a last interglacial charcoal and burnt stone feature: is it a hearth? *Proceedings of the Royal Society of Victoria*, this volume.
- Miller, C.R., James, N.P. & Kyser, T.K., 2013. Genesis of blackened limestone clasts at late Cenozoic subaerial exposure surfaces, southern Australia. *Journal of Sedimentary Research* 83: 339–353.
- Moropoulou, A., Bakolas, A. & Aggelakopoulou, E., 2001. The effects of limestone characteristics and calcination temperature to the reactivity of the quicklime. *Cement and Concrete Research* 31(4): 633–636.
- Murray-Wallace, C.V., 2002. Pleistocene coastal stratigraphy, sea-level highstands and neotectonism of the southern Australian passive continental margin – a review. *Journal of Quaternary Science* 17: 469–489.
- Murray-Wallace, C.V. & Woodroffe, C.D. 2014. *Quaternary Sea-Level Changes: A Global Perspective*. Cambridge University Press, Cambridge, 484 pp.
- Mullins, C.E., 1977. Magnetic susceptibility of the soil and its significance in soil science — a review. *Journal of Soil Science* 28: 223–246.
- Nair, H. & Sherwood, J., 2007. An unusual shell bed at Point Ritchie, Warrnambool, Victoria — predator midden or natural shell bed? *Proceedings of the Royal Society of Victoria* 119(1): 69–86.
- O’Connell, J.F., Allen, J., Williams, M.A.J., Williams, A.N., Turney, C.S.M., Spooner, N.A., Kamminga, J., Brown, G. & Cooper, A. 2018. When did *Homo sapiens* first reach Southeast Asia and Sahul? *Proc. Natl. Acad. Sci. USA* 34: 8482–8490.
- Oldfield, F. & Crowther J., 2007. Establishing fire incidence in temperate soils using magnetic measurements. *Palaeogeography, Palaeoclimatology, Palaeoecology* 249: 362–369.
- Peters, C. & Thompson, R., 1999. Supermagnetic enhancement, superparamagnetism, and archaeological soils. *Geoarchaeology* 14: 401–413.
- Railsback, L.B., Gibbard, P.L., Head, M.J., Voarintsoa, N.R.G. & Toucanne, S., 2015. An optimized scheme of lettered marine isotope substages for the last 1.0 million years, and the climatostratigraphic nature of isotope stages and substages. *Quaternary Science Reviews* 111: 94–106.
- Reeckmann, S.A. & Gill, E.D., 1981. Rates of vadose diagenesis in Quaternary dune and shallow marine calcarenites, Warrnambool, Victoria, Australia. *Sedimentary Geology* 30: 157–172.

- Sherwood, J.E., Barbetti, M., Ditchburn, R., Kimber, R.W.L., McCabe, W., Murray-Wallace, C.V., Prescott, J.R. & Whitehead, N., 1994. A comparative study of Quaternary dating techniques applied to sedimentary deposits in southwest Victoria, Australia. *Quaternary Science Reviews* 13: 95–110.
- Sherwood, J., Oyston, B. and Kershaw, A.P., 2004. The age and contemporary environments of Tower Hill Volcano, southwest Victoria, Australia. *Proceedings of the Royal Society of Victoria* 116: 69–76.
- Sherwood, J.E., McNiven, I. J., & Laurensen, L., 2018a. The Moyjil site, south-west Victoria, Australia: shells as evidence of the deposit's origin. *Proceedings of the Royal Society of Victoria*, this volume.
- Sherwood, J.E., Bowler, J.M., Carey, S.P., Hellstrom, J., McNiven, I.J., Murray-Wallace, C.V., Prescott, J.R., Questiaux, D.G., Spooner, N.A., Williams, F.M. & Woodhead, J.D., 2018b. The Moyjil site, south-west Victoria, Australia: chronology. *Proceedings of the Royal Society of Victoria*, this volume.
- Shinn, E.A. & Lidz, B.H., 1988. Blackened limestone pebbles: Fire at subaerial unconformities. In *Paleokarst*, Choquette, P.W. and James, N.P., eds. New York, Springer-Verlag, pp. 117–131.
- VandenBerg, A.H.M., 2009. Rock unit names in the Bendigo zone portion of central Victoria, Seamless Geology Project. *Geological Survey of Victoria Report* 129, 112 pp.